JOURNAL OF SPACECRAFT AND ROCKETS
Vol. 47, No. 6, November–December 2010

Predictive Nutation and Spin Inversion Control of Spin-Stabilized Spacecraft

Hyun-Sam Myung* and Hyochoong Bang†
Korea Advanced Institute of Science and Technology, Daejeon 305-701, Republic of Korea

DOI: 10.2514/1.48336

Thus far, nutation control and spin inversion maneuvers have been treated from different perspectives for the stabilization of spinning spacecraft. This paper tackles these problems in a unified framework by applying a predictive control for minor-axis spinners with a transverse wheel. Predictive control seeks a control input minimizing a cost function in the form of the weighted sum of predicted output and control effort. The two-step design approach of the proposed application defines the cost as 1) angular momentum only on the orthogonal plane to the minor axis and 2) angular momentum augmenting the error of the desired minor axis. Corresponding weight parameters are designed based upon physical meanings, and a final desired state or online time-varying trajectory is suggested as a reference for successful and effective control. Both control laws are shown to be essentially globally stable about the minor-axis spin, including flat-spin recovery. However, while the final polarity of the first is unpredictable, the second is capable of spin direction control enabling inversion maneuvers. Simulation results also verify robustness of the proposed controllers against assumable system uncertainties.

Nomenclature

$\boldsymbol{a}$	=	reaction wheel axis vector
B	=	spacecraft body frame; $(\boldsymbol{b}_1, \boldsymbol{b}_2, \boldsymbol{b}_3)$
c	=	nonlinear output function of x
$c\theta$	=	$\cos\theta$
e_M, e_{M1}, e_{M2}	=	predictive control input voltages for systems in general and of relative degrees 1 and 2, V
$e_{\max}$, $e_{\min}$	=	maximum and minimum input voltages, V
f, g	=	nonlinear system and control transition functions of x
$\boldsymbol{H}$, H	=	angular momentum and angular momentum magnitude, kg · m^2/s
h	=	prediction time step, s
I_B	=	total moment of inertia of the spacecraft and the wheel except for $K\boldsymbol{a}$; diag(I_1, I_2, I_3), kg · m^2
$I(t)$	=	characteristic parameter, kg · m^2
J, J_1, J_2	=	predictive control cost functions for systems in general and of relative degrees 1 and 2
K	=	wheel moment of inertia about the $\boldsymbol{a}$ axis, kg · m^2
L	=	Lie derivative
N	=	wheel motor torque constant, N · m/A
Q, Q_1, Q_2	=	predictive control output weight matrices for systems in general and of relative degrees 1 and 2
R	=	armature resistance, Ω
$r(\subset R^n)$	=	output reference trajectory
$s\theta$	=	$\sin\theta$
T	=	kinetic energy, N · m
t	=	time, s
$u(\subset R^p)$	=	control input vector
W, w	=	control input weight matrix and transformed control input weight parameter
$x(\subset R^m)$	=	state variable vector
$y(\subset R^n)$	=	output vector
z	=	nonlinear function
α_i	=	linear control feedback coefficients, i is equal to 1, 2, and 4
γ	=	relative degree
$\Delta\omega_3$	=	ω_3-$\omega^h_{3\text{ref}}$
$\boldsymbol{\eta}$	=	vector normal to $\boldsymbol{\sigma}$; $(\eta_1, \eta_2, \eta_4)^T$
θ	=	reaction wheel alignment angle from $\boldsymbol{b}_1$ axis, rad
κ	=	linear control feedback gain
Λ	=	nonlinear function
μ_i, ν_i	=	equilibrium point solutions, i is equal to 1 and 4
$\boldsymbol{\sigma}$,	=	$(\sigma_1, \sigma_2, \sigma_4)^T$
σ_i	=	equilibrium points; i is equal to 1 to 4
Φ	=	closed-loop system matrix except for ω_3
φ	=	nutation angle, rad
Ω	=	absolute rotating speed of the wheel, rad/s
$\boldsymbol{\omega}$	=	body angular velocity vector, rad/s; $(\omega_1, \omega_2, \omega_3)^T$
ϖ	=	relative rotating speed of the wheel with respect to the spacecraft, rad/s
$\omega^{\text{cp}}_{3\text{ref}}$	=	$\omega_{3\text{ref}}$ using the characteristic parameter
$\omega^h_{3\text{ref}}$	=	$\omega_{3\text{ref}}(t+h)$

Subscripts

b	=	body
f	=	final state
ref	=	reference
true	=	true parameter values
0	=	initial condition

I. Introduction

WHEN a spinning body is required to be aligned along a certain desired direction, one main concern is the degree of misalignment, known as nutation. The objective of nutation control of spin-stabilized spacecraft is to control the spacecraft to spin about a desired body axis by reducing the nutation angle to zero.

Spins about major and minor axes are dynamically stable, while intermediate axis spin is unstable [1]. In the presence of energy dissipation, however, only the major-axis spin is stable, which means that minor and intermediate axis spinners require an active control to stabilize while the major spinner usually adopts a passive damper when faster nutation damping is desired via aggressive energy dissipation. The single-axis spin stabilization method has restricted applications, since a spinning spacecraft offers limited mission diversity. Because of its simplicity and low cost, however, spin stabilization attitude control is still employed in small spacecraft applications and upper stage orbit insertion maneuvers [2].

Received 1 December 2009; revision received 6 July 2010; accepted for publication 20 July 2010.

*Graduate Student, Division of Aerospace Engineering, 335 Gwahangno, Yuseong-Gu.

†Professor, Division of Aerospace Engineering, 335 Gwahangno, Yuseong-Gu. Senior Member AIAA.

From the perspective of control simplicity, major-axis spin may be favored. Meanwhile, minor-axis spin is advantageous, since prolate arrangement of spacecraft in a launch vehicle is more volume effective. Also, minor spin is proper and preferred if long payloads such as cameras and antenna necessitate their alignment in the spin direction. In this case, spin polarity, which can be either parallel or antiparallel, is important for payload operation. It is also noteworthy that a spin inversion maneuver can extend the lifetime of satellites by protecting payloads and structures from solar radiation by periodically inverting their exposed faces [3–5]. Furthermore, if spin inversion can be performed by a momentum storage device such as a reaction wheel, then the huge fuel expenditures necessary to achieve spin inversion through the use of thrusters may be avoided [6].

Prior works have treated nutation control and spin inversion separately. Devey et al. [7] solved when and how thrusters should be fired for nutation control spinning about the minor axis, assuming the nutation angle was very small. Reference [8] used a single transverse wheel to affect spin about the intermediate axis using a linear feedback control law. In addition to classical linear controls, a variety of nonlinear control theories such as feedback linearization [9], artificial neural networks [10], and backstepping control [11] have been applied to achieve momentum transfer control about the minor axis from the body to a reaction wheel. Marshall and Tsiotras [12] treated angular velocity stabilization using a single-gimbal variable-speed control moment gyro (VSCMG). The Lyapunov-based state feedback control globally asymptotically stabilized the spacecraft system. However, adopting a VSCMG took advantage of two degrees of freedom in generating control input. Zhang et al. [13] solved spin-axis stabilization of spacecraft under sinusoidal disturbance torques. However, thrusters were facilitated as actuators in two axes. Holden and Lawrence in [14] and Lawrence and Holden [2] explored nutation control of spin-stabilized spacecraft with a single transverse reaction wheel via the Lyapunov approach. Except in very narrow unstable regions, the Lyapunov control was shown to be essentially globally stable. However, it was mentioned that an inverted turn was not avoidable, depending on how the state trajectory left the unstable equilibrium. The solution in [2] is essentially swapping and rotating the equilibrium points, thus rendering the approach incapable of distinguishing an inverted turn from a noninverted one still having two stable equilibria.

Spin inversion control, which achieves a 180° nutation angle relative to the initial orientation, can be pursued both as a solution to resolve the issue preventing the inverted turn in nutation control and as one of the large angle orientation control maneuvers. Rahn and Barba [5] investigated spin orientation control by thruster firing while spin axis changed from the minor to the major axes. Beachley and Uicker [3] and Beachley [4] proposed a satellite inversion system that rearranged the mass property of a spacecraft with the possibility of mechanical malfunction or induced jitter in the spacecraft body. Utilization of a reaction wheel for spin inversion control is highly advantageous in terms of fuel consumption, launch cost, operational life, and maintaining a low level of induced disturbances [6]. Fong proposed, in [6], a spin inversion control scheme that operated via the product of inertia coupling of a mounted rotor, but the intentional asymmetry of the rotor may give rise to undesired additional nutational motion of the body. Based on the development in [8], which makes use of the directional instability of an intermediate axis, Fowell [15] disclosed a spin inversion control law using a transverse reaction wheel rotating about an intermediate axis. However, the intermediate axis has hardly been selected for the vehicle spin axis.

The dynamics of the spinning spacecraft with a reaction wheel are closely related to that of the dual-spin spacecraft. Even though the dynamics of a spinning body are a classical problem, many researchers have investigated the dynamics of gyrostats consisting of two rigid bodies: spinup dynamics [16], resonant motion [17], escape from trapped states [18,19], etc. The resonant motion of a spinning body is a residual nutational motion due to imbalance of a rigid body or thruster firing. Resonance capture or trapped states are large angle nutational motions similar to the flat spin. Most difficulties in finding analytic solutions of dual-spin spacecraft arise from uncertainties and dynamic complexities such as inertia asymmetry and small rotor imbalance. How to find equilibrium points and periodic solutions by numerical continuation methods were also presented in [20,21]. These results revealed a better understanding about characteristics of dual-spin spacecraft. However, there is still a need for implementing a closed-loop control law.

A predictive control approach is applied in order to solve the essentially globally stable nutation control problem. Lu first devised a nonlinear predictive control for continuous systems [22] using nonlinear function approximation. Thereafter, predictive control has successfully been applied to nonlinear control problems [23–25]. It provides a real-time reference tracking control, and it shares the same properties with feedback linearization in an ideal case. It is also a suboptimal control for only a designed prediction horizon. Predictive control enables us to deal with the nutation control as a nonlinear feedback control.

Based on a predictive control approach, this study provides a unified solution for nutation control and spin orientation control simultaneously through corresponding reference trajectories using a single transverse reaction wheel. Various predictive nutation control laws can be established by properly selecting design parameters such as output variables, reference trajectories, control and output weights, and the prediction time step. By designing the cost function in terms of angular momentum error with respect to a desired reference condition, the proposed nonlinear feedback control law can excite the system periodically to recover from the flat spin or to escape from unwanted spin orientation for a transition to a desired axis spin. Rendering only one desired equilibrium stable among six and rendering others unstable guarantees essentially global asymptotical stability without unwanted inverted turns. This is an important part of successful spin inversion that distinguishes this paper from the previous works. Analysis of closed-loop equilibrium points is also presented in order to verify the essential global stability.

This paper is organized as follows: spacecraft dynamics and problem description are briefly introduced in Sec. II, and a review of predictive control is presented in Sec. III. Section IV shows how to solve nutation control using the predictive control approach by designing control parameters minimizing body angular momentum and appropriate reference trajectories in two design steps. Equilibrium points of the closed-loop system for each control law are found, and the stability of the equilibrium points is investigated. Examples for flat-spin recovery and the spin inversion maneuver are also illustrated in Sec. IV to verify the proposed control laws via numerical simulations.

II. Spacecraft Dynamics

In this study, we deal with nutation control using a single transverse reaction wheel [2]. Among the spacecraft body frame axes, $\boldsymbol{b}_3$ is assumed as a minor principal axis. A reaction wheel is mounted on the spacecraft and is aligned in a direction with θ from the $\boldsymbol{b}_1$ axis on the $\boldsymbol{b}_1\boldsymbol{b}_2$ plane, as illustrated in Fig. 1. The vector $\boldsymbol{a}$ is assumed to not be parallel with any of the principal axes.

The total angular momentum of the spacecraft and the wheel is given in the form

$$\boldsymbol{H} = I_B\boldsymbol{\omega} + K\Omega\boldsymbol{a} \tag{1}$$

where the relationship of the absolute wheel speed and the relative wheel speed with respect to the spacecraft is

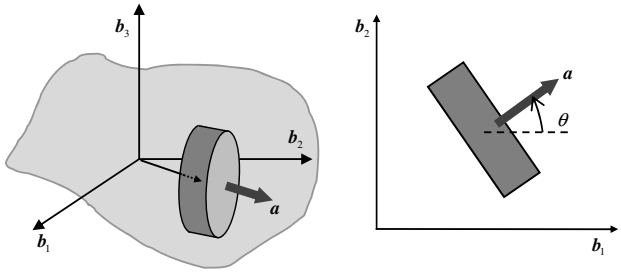

Fig. 1 Spacecraft body axes and reaction wheel alignment.

$$\Omega = \boldsymbol{\omega} \cdot \boldsymbol{a} + \varpi \tag{2}$$

The rotational kinetic energy of the system is expressed as [26]

$$T = \tfrac{1}{2}\boldsymbol{\omega}^T I_B \boldsymbol{\omega} + \tfrac{1}{2} K \Omega^2 \tag{3}$$

Assuming there is no external torque, the total angular momentum is conserved according to the angular momentum principle, which can be expressed such that

$$\mathbf{0} = \frac{\mathrm{d}}{\mathrm{d}t}\boldsymbol{H} = \frac{{}^{B}\mathrm{d}}{\mathrm{d}t}\boldsymbol{H} + \boldsymbol{\omega} \times \boldsymbol{H}$$

In terms of body angular velocity vector,

$$\dot{\boldsymbol{\omega}} = -I_B^{-1}[\boldsymbol{\omega} \times (I_B \boldsymbol{\omega} + K\Omega \boldsymbol{a}) + K\dot{\Omega}\boldsymbol{a}] \tag{4}$$

The reaction wheel is assumed to be controlled by a voltage-fed permanent-magnet dc motor [27], so we have

$$K\dot{\Omega} = -\frac{N^2}{R}\varpi + \frac{N}{R}e_M \tag{5}$$

Therefore, the input voltage e_M is a scalar control input. It is assumed that the input voltage is saturated such that

$$\mathrm{sat}\,(e_M) = \begin{cases} e_{\max} & \text{for } e_M \geq e_{\max} \\ e_{\min} & \text{for } e_M \leq e_{\min} \end{cases} \tag{6}$$

Equations (4) and (5) with the relationship (2) constitute the equation of motion of spacecraft for nutation control. By the first term in Eq. (5), energy is dissipated by the motor armature resistance [2]. The spacecraft equations of motion in Eqs. (4) and (5) are rewritten as

$$\begin{bmatrix} \dot{\boldsymbol{\omega}} \\ \dot{\Omega} \end{bmatrix} = \begin{bmatrix} -I_B^{-1}\left\{\boldsymbol{\omega} \times (I_B\boldsymbol{\omega} + K\Omega\boldsymbol{a}) + \frac{N^2}{R}(\boldsymbol{a}\boldsymbol{a}^T)\boldsymbol{\omega} - \frac{N^2}{R}\Omega\boldsymbol{a}\right\} \\ \frac{N^2}{KR}\boldsymbol{\omega}^T\boldsymbol{a} - \frac{N^2}{KR}\Omega \end{bmatrix} + \begin{bmatrix} -I_B^{-1}\frac{N}{R}\boldsymbol{a} \\ \frac{N}{KR} \end{bmatrix} e_M \tag{7}$$

In a scalar form,

$$\begin{aligned} I_1\dot{\omega}_1 &= (I_2 - I_3)\omega_2\omega_3 + Ks\theta\omega_3\Omega + \frac{N^2 c\theta}{R}\varpi - \frac{Nc\theta}{R}e_M \\ &= I_1 f_1 + I_1 g_1 e_M \\ I_2\dot{\omega}_2 &= (I_3 - I_1)\omega_3\omega_1 - Kc\theta\omega_3\Omega + \frac{N^2 s\theta}{R}\varpi - \frac{Ns\theta}{R}e_M \\ &= I_2 f_2 + I_2 g_2 e_M \\ I_3\dot{\omega}_3 &= (I_1 - I_2)\omega_1\omega_2 + K\Omega(c\theta\omega_2 - s\theta\omega_1) = I_3 f_3 \\ K\dot{\Omega} &= -\frac{N^2}{R}\varpi + \frac{N}{R}e_M = Kf_4 + Kg_4 e_M \end{aligned} \tag{8}$$

where

$$\Omega = \varpi + \omega_1 c\theta + \omega_2 s\theta \tag{9}$$

It is assumed that $I_1 > I_2 (> I_3)$ in order to cover spacecraft with asymmetric axes without loss of generality. For the purpose of numerical verification of the analyses, each parameter assumed is listed in Table 1 [2].

Now, the desired final state of nutation and spin inversion control about the minor axis from an arbitrary initial condition is specified by

$$(\omega_1, \omega_2, \omega_3, \Omega)_f^T = (0, 0, \omega_{3f}, 0)^T \tag{10}$$

Table 1 An example of spacecraft parameters

Parameter	Value, kg m^2	Parameter	Value
I_1	8.1942	θ	0.4398 rad
I_2	6.9718	N	0.1 Nm/A
I_3	4.6130	R	0.5Ω
K	0.0077		

Nutation is a general term describing a rotational motion that the instantaneous rotation axis of the body is not aligned with a principal axis [1]. Recovery from flat spin and inversion of spin direction are special but extreme cases of nutation control. The nutation angle for the $\boldsymbol{b}_3$ axis as the reference is defined by

$$\varphi = \cos^{-1}\frac{I_3\omega_3}{H_b}$$

Since the reference axis in this study is the minor axis, the major-axis spin (or a flat spin) and a spin about the intermediate axis are undesired states. Even though the nutation angle is a widely used measure quantifying the magnitude of a nutational motion, it is not appropriate to discriminate flat-spin states. Spins about each principal axis are classified by the ratio of the angular momentum and the rotational kinetic energy: namely, a characteristic parameter [5,26]

$$I(t) = \frac{H_b^2}{2T_b}; \qquad [I_3 \leq I(t) \leq I_1] \tag{11}$$

If $I(t) > I_2$, the vehicle is in a flat-spin condition. Recovery from the flat spin implies in this problem $I(t)$ decreases less than the bifurcation value I_2, and it becomes closer to I_3. $I(t)$, however, is identical for both positive and negative spins. Therefore, the nutation angle or the sign of ω_3 must be taken into account in order to deal with inversion of the spinning direction from the unwanted negative or positive spin to the desired polarity. Figure 2 illustrates a family of angular momentum traces, polhodes, and the spin states of a rigid body with the moment of inertia in Table 1 on the momentum sphere. The polhodes of the spacecraft body will be open paths under the interaction with the reaction wheel.

III. Review of Predictive Control

Predictive control is first briefly reviewed in this section before applied to the nutation control problem. This approach is basically a high gain feedback control obtained by approximate nonlinear function expansions similar to feedback linearization. The feedback linearization approach assumes a perfectly known system model so that the control input has no proper physical meaning under conditions of model uncertainty and control input saturation. Meanwhile,

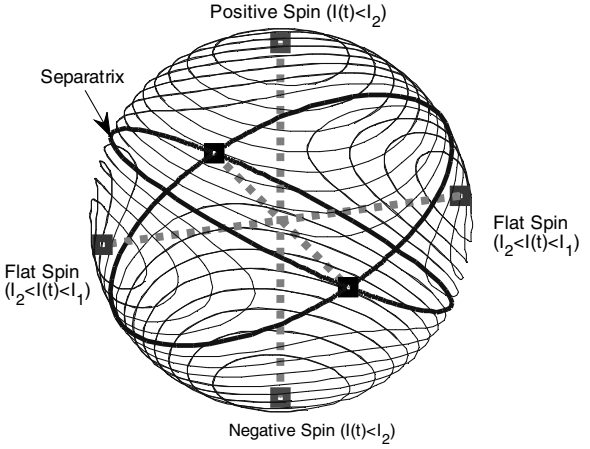

Fig. 2 Polhodes (solid lines) and spin states on the momentum sphere with principal axis spins (squares).

predictive control is known to have obviousness and robustness, even in those cases.

Let us assume a nonlinear system such as

$$\dot{x}(t) = f[x(t)] + g[x(t)]u(t); \qquad y(t) = c[x(t)] \tag{12}$$

This system is affine in control input $u(t)$. The objective of predictive control is to make the output of the system follow a predesigned reference trajectory $r(t)$ by designing an appropriate control input $u(t)$. The control $u(t)$ is determined by minimizing the cost function in the form of the weighted sum of the predicted output error at time $t + h$ and the control effort, such as

$$J[x(t), u(t)] = \tfrac{1}{2}[y(t+h) - r(t+h)]^T Q[y(t+h) - r(t+h)] + \tfrac{1}{2}u^T(t)Wu(t) \tag{13}$$

where $Q \geq 0$, $W \geq 0$, and $h > 0$.

Output weight matrix Q may serve as an output selector by assigning zero to proper diagonal elements. To determine $u(t)$, $r(t + h)$ and $y(t + h)$ should be provided. While $r(t + h)$ is supposed to be a predesigned function, $y(t + h)$ should be properly predicted. Since the cost function is in a quadratic form of the predicted output, it is a convex function of the control input if the predicted output is linearly expressed by the control input. Since the predicted output is not yet actually produced, it may be predicted best by using its model in Eq. (12). Therefore, the predicted output is approximated in an affine form with respect to the control input. Let us first define a relative degree $\gamma_i (i = 1, \ldots, n)$ as the order of differentiation of output $y_i(t)$ until it is first written in terms of $u(t)$. Unless there are zero dynamics, the relative degree always exists because the system is assumed to be affine. However, each relative degree for each output component may be different. By Taylor series expansions of the output to the relative degree using the Lie derivative, we have

$$y_i(t+h) \approx y_i(t) + \sum_{j=1}^{\gamma_i} \frac{h^j}{j!}\frac{\mathrm{d}^j}{\mathrm{d}t^j} y_i(t) \approx y_i(t) + z_i[x(t), h] + \Lambda_i[x(t), h]u(t); \qquad i = 1, 2, \cdots, n \tag{14}$$

where

$$z_i = \sum_{j=1}^{\gamma_i} \frac{h^j}{j!} L_f^j(c_i); \qquad L_f^j(c_i) = c_i \quad \text{for } j = 0;$$

$$L_f^j(c_i) = \frac{\partial L_f^{j-1}(c_i)}{\partial x} f \quad \text{for } j \geq 1;$$

$$\Lambda_i[x(t), h] = \frac{h^{\gamma_i}}{\gamma_i!}\{L_{g_1}[L_f^{\gamma_i - 1}(c_i)], \cdots, L_{g_p}[L_f^{\gamma_i - 1}(c_i)]\};$$

$$L_{g_k}[L_f^{\gamma_i - 1}(c_i)] = \frac{\partial L_f^{\gamma_i - 1}}{\partial x} g_k; \qquad k = 1, \cdots, p$$

and g_k is the kth column of $g(x)$.

By inserting Eq. (14) into Eq. (13), we obtain a quadratic cost function in terms of control $u(t)$. We can find the optimal control solution by $\mathrm{d}J/\mathrm{d}u = 0$ as

$$u(t) = -\{\Lambda^T Q \Lambda + W\}^{-1}\{\Lambda^T Q[y(t) - z[x(t), h] - r(t+h)]\} \tag{15}$$

Now, one-step-ahead predictive control is applied to nutation control problems in the following section.

IV. Predictive Nutation Control

Comparing Eq. (7) with Eq. (12), it follows that

$$f = \begin{bmatrix} -I_B^{-1}\left\{\boldsymbol{\omega} \times (I_B\boldsymbol{\omega} + K\Omega\boldsymbol{a}) + \frac{N^2}{R}(\boldsymbol{a}\boldsymbol{a}^T)\boldsymbol{\omega} - \frac{N^2}{R}\Omega\boldsymbol{a}\right\} \\ \frac{N^2}{KR}\boldsymbol{\omega}\cdot\boldsymbol{a} - \frac{N^2}{KR}\Omega \end{bmatrix}$$

$$g = \begin{bmatrix} -I_B^{-1}\frac{N}{R}\boldsymbol{a} \\ \frac{N}{KR} \end{bmatrix} \tag{16}$$

From Eq. (16), the relative degree γ_i ($i = 1, 2, 4$) is equal to 1. Since the wheel lies on the $\boldsymbol{b}_1\boldsymbol{b}_2$ plane, the relative degree between ω_3 and $e_M(t)$ is equal to two. Selection of the output, therefore, will result in different control characteristics. In this section, we design and analyze nutation control laws by two steps: 1) using only outputs of the relative degree 1 and 2) using all four outputs, including ω_3 of the relative degree 2.

A. Design Step 1: Using Only Outputs of the Relative Degree 1

A strategy to select weight parameters is the key to implementing the predictive nutation control. How to design the weight matrices was not clearly addressed in the predictive control theory and application studies [22–25]. This study proposes output and control weight selection based on the dynamic characteristics of a spinning body. Spins about each principal axis possess different kinetic energy levels for the same magnitude of angular momentum. Since minor-axis spin has the highest energy level and major-axis spin has the lowest, minor-axis spin can be achieved by providing more kinetic energy to the body. It may be realized by finding the control input maximizing the rotational energy of the body, or the opposite strategy may be adopted to design a control input minimizing the body angular momentum. Since a reaction wheel is the only actuator assumed in the absence of external torques, the body angular momentum may change while the total angular momentum is conserved. Therefore, the second approach is also applicable. According to the predictive control strategy, we seek to minimize the angular momentum other than the desired minor axis by defining $y = (\omega_1, \omega_2, \Omega)^T$, $r(t) = (0, 0, 0)^T$, and

$$Q_1 = \begin{bmatrix} I_1^2 & 0 & 0 \\ 0 & I_2^2 & 0 \\ 0 & 0 & K^2 \end{bmatrix}$$

As a result, the cost function in Eq. (13) becomes

$$J_1 = \tfrac{1}{2}[\{I_1\omega_1(t+h)\}^2 + \{I_2\omega_2(t+h)\}^2 + \{K\Omega(t+h)\}^2 + We_M^2] \tag{17}$$

which minimizes the angular momentum of the body in the transverse direction with a minimum control input.

Note that W works as an alleviating parameter of control energy. If $W = 0$, the inverse of the prediction time step h becomes an output error feedback gain [22]. Otherwise, the ratio of W to h eases the feedback gain. To make the effects of W and h clearer, we attempt to redefine W as

$$W = h^2\frac{N^2}{R}w; \qquad w \geq 0 \tag{18}$$

where w is nondimensional. This transformation is reasonable, since the longer the prediction step, the less control effort is necessary, which implies that a larger$W$ is required.

Accordingly, the predictive control law in Eq. (15) is obtained as

$$e_{M1}(t) = -\frac{R}{(w+2)N}\left[\frac{1}{h}(-I_1\omega_1 c\theta - I_2\omega_2 s\theta + K\Omega) + \left\{-(I_2 - I_3)\omega_2\omega_3 c\theta + (I_1 - I_3)\omega_1\omega_3 s\theta - \frac{2N^2}{R}\varpi\right\}\right] \tag{19}$$

In Eq. (19), the control input consists of two parts: the first-order and the second-order feedback terms, among which h determines only how much the first-order terms are fed back. The longer the prediction step, the less the first-order terms are fed back, since linear approximation becomes less accurate. Therefore, the amount of the nonlinear second-order feedback becomes larger than that of the first order. On the other hand, the control weight parameter w adjusts the overall control scale. Selecting appropriate w avoids an excessive control input being delivered to the system when a small prediction step may induce unnecessary control effort. The combination of the first-order and the second-order terms essentially constitutes a proportional and differential feedback control with the time constant h. Consequently, its convergence speed is faster than that of the linear feedback only. Apparently, ω_3 in the second-order terms accelerates spin transition due to the conservation of the total angular momentum.

Note that the definition of the cost function in Eq. (17) is incapable of distinguishing the sign of ω_3. Therefore, it is predictable that recovery from a flat spin will be possible, but an inverted turn may be unavoidable, as the Lyapunov-based linear feedback control established by Lawrence and Holden in [2]. This issue is resolved by augmenting the cost function with the ω_3 prediction later in the next section. Let us refer to the control law in Eq. (19) as PNC1 (predictive nutation controller 1) hereafter.

1. *Stability Analysis of the Control Law*

When a dynamic system is fully actuated (i.e., when $n = p$), the dynamics of the closed-loop system of the output error under the predictive control law in Eq. (15) with $W = 0$ are ideally rearranged with stable polynomials. This nutation control system, however, has $n > p$, so that the closed-loop dynamics are rather complicated. For stability analysis of the closed-loop system with PNC1, the equilibrium points are obtained by solving Eqs. (4) and (5):

$$\boldsymbol{\omega} \times \boldsymbol{H} = 0 \tag{20}$$

$$e_M - N\varpi = 0 \tag{21}$$

Assuming a nonzero angular momentum, $\boldsymbol{\omega}$ and $\boldsymbol{H}$ are parallel vectors [28], and the wheel is stuck in balance between the dissipated energy and the voltage input for nontrivial solutions. Since Eqs. (20) and (21) are expanded in a complicated form, we seek to obtain the equilibrium points in two steps: 1) $\omega_3 = 0$ and 2) $\omega_3 \neq 0$ for the initially given angular momentum magnitude H_0.

For step 1, substituting $\omega_3 = 0$ into Eq. (20) reduces in terms of σ_i to

$$(I_1 - I_2)\sigma_1\sigma_2 + K\sigma_4(\sigma_2 c\theta - \sigma_1 s\theta) = 0 \tag{22}$$

Equation (21) is also simplified as

$$\boldsymbol{\eta} \cdot \boldsymbol{\sigma} = 0 \tag{23}$$

where

$$\boldsymbol{\eta} = \left[\left(\frac{I_1}{h} + \frac{wN^2}{R}\right)c\theta, \left(\frac{I_2}{h} + \frac{wN^2}{R}\right)s\theta, -\left(\frac{K}{h} + \frac{wN^2}{R}\right)\right]^T$$

which always yields two different real roots with the two solutions denoted as $\sigma_i = \mu_i\sigma_2$ and$\sigma_i = \nu_i\sigma_2$ $(i = 1, 4)$, respectively. Finally, four equilibria are obtained: $\pm(\mu_1\sigma_2, \sigma_2, 0, \mu_4\sigma_2)^T$ and $\pm(\nu_1\sigma_2, \sigma_2, 0, \nu_4\sigma_2)^T$, where σ_2 is determined by the angular momentum constraint of the given H_0.

For step 2), we can establish a closed-loop system equation by substituting Eq. (19) into Eq. (8) that, except for the third equation, constitutes linear dynamics for which the system matrix contains ω_3:

$$\begin{aligned} I_1\dot{\omega}_1 = {} & \left\{(I_1 - I_3)\frac{c\theta s\theta}{w+2}\omega_3 - \frac{c^2\theta}{h(w+2)}I_1 - \frac{N^2c^2\theta}{R}\frac{w}{w+2}\right\}\omega_1 \\ & + \left\{(I_2 - I_3)\left(1 - \frac{c^2\theta}{w+2}\right)\omega_3 - \frac{c\theta s\theta}{h(w+2)}I_2 \right. \\ & \left. - \frac{N^2c\theta s\theta}{R}\frac{w}{w+2}\right\}\omega_2 + \left\{Ks\theta\omega_3 + \frac{c\theta}{h(w+2)}K \right. \\ & \left. + \frac{N^2c\theta}{R}\frac{w}{w+2}\right\}\Omega \end{aligned} \tag{24}$$

$$\begin{aligned} I_2\dot{\omega}_2 = {} & \left\{-(I_1 - I_3)\left(1 - \frac{s^2\theta}{w+2}\right)\omega_3 - \frac{c\theta s\theta}{h(w+2)}I_1 \right. \\ & \left. - \frac{N^2c\theta s\theta}{R}\frac{w}{w+2}\right\}\omega_1 + \left\{-(I_2 - I_3)\frac{c\theta s\theta}{w+2}\omega_3 - \frac{c\theta s\theta}{h(w+2)}I_2 \right. \\ & \left. - \frac{N^2s^2\theta}{R}\frac{w}{w+2}\right\}\omega_2 + \left\{-Kc\theta\omega_3 + \frac{s\theta}{h(w+2)}K \right. \\ & \left. + \frac{N^2s\theta}{R}\frac{w}{w+2}\right\}\Omega \end{aligned} \tag{25}$$

$$I_3\dot{\omega}_3 = (I_1 - I_2)\omega_1\omega_2 + K\Omega(\omega_2 c\theta - \omega_1 s\theta) \tag{26}$$

$$\begin{aligned} K\dot{\Omega} = {} & \left\{-(I_1 - I_3)\frac{s\theta}{w+2}\omega_3 + \frac{c\theta}{h(w+2)}I_1 + \frac{N^2c\theta}{R}\frac{w}{w+2}\right\}\omega_1 \\ & + \left\{(I_2 - I_3)\frac{c\theta}{w+2}\omega_3 + \frac{s\theta}{w+2}I_2 + \frac{N^2s\theta}{R}\frac{w}{w+2}\right\}\omega_2 \\ & + \left\{-\frac{1}{h(w+2)}K - \frac{N^2}{R}\frac{w}{w+2}\right\}\Omega \end{aligned} \tag{27}$$

Equations (24), (25), and (27) can be expressed in the form of $\mathbf{0} = \Phi(\omega_3)\boldsymbol{\sigma}$. Eigenvalue analysis indicates that Φ has nonzero eigenvalues and is invertible only if $\omega_3 \neq 0$, so that $\boldsymbol{\sigma} = \mathbf{0}$ and $\sigma_3 = H_0/I_3$ under the angular momentum constraint. Therefore, $(0, 0, \pm H_0/I_3, 0)^T$ are also equilibrium points.

From steps 1 and 2, there are six equilibrium points, among which the four equilibria found in step 1 are all unstable, and the other two are stable. The characteristic equation of Φ has at least one of the nonnegative eigenvalues when

$$0 \leq \omega_3 \leq \frac{(I_1 - I_2)I_3 c\theta s\theta}{h\{w(I_1 - I_3)(I_2 - I_3) + 2I_1I_2 - (1 + c^2\theta)I_1I_3 - (1 + s^2\theta)I_2I_3 + I_3^2\}} \tag{28}$$

Then, combining Eqs. (22) and (23), it follows that

$$\begin{aligned} & \sigma_1^2\left(\frac{I_1}{h} + \frac{wN^2}{R}\right) + \frac{\sigma_1\sigma_2}{c\theta s\theta}\left\{-\left(\frac{I_1}{h} + \frac{wN^2}{R}\right)c^2\theta + \left(\frac{I_2}{h} + \frac{wN^2}{R}\right)s^2\theta \right. \\ & \left. + \frac{I_1 - I_2}{K}\left(\frac{K}{h} + \frac{wN^2}{R}\right)\right\} - \sigma_2^2\left(\frac{I_2}{h} + \frac{wN^2}{R}\right) = 0 \end{aligned}$$

so that the equilibrium points on the boundary are unstable, as verified by numerical simulations later. For the parameter values of Table 1, the region in Eq. (28) is a very thin strip. For applicable values of h and w, for instance, when $h = 6$ s and $w = 4$, $0 \leq \omega_3 \leq 0.0058$ rad/s.

On the other hand, in the subtracted region of Eq. (28), the characteristic equation results in a stable polynomial $\boldsymbol{\sigma} = \mathbf{0}$ being a

stable equilibrium, so that the equilibria $(0, 0, \pm H_0/I_3, 0)^T$ are stable. Thus, only the minor-axis spins, including positive and negative spins, are stable.

It is noticeable that the larger the h and w, the thinner the instability strip. In other words, larger parameters broaden the stable region as well as slow down the convergence speed. The unstable region can be escaped from under various types of disturbing torques, as discussed in [2]. This results in essentially global convergence to stable equilibrium points.

2. *Numerical Examples*

For understanding the behaviors and characteristics of the closed-loop system with PNC1, numerical examples are introduced. Simulation parameters are given in Table 1, and the control voltage saturation is $e_{\max} = 10$ V and $e_{\min} = -10$ V. The predictive control parameters are specified as $h = 6.0$ s and $w = 6.0$. First, cases with initial conditions starting near the four undesired closed-loop equilibrium points are simulated. The equilibria for the specified parameters are obtained as

$$\pm\,(1.7739, 0.0712, 0.0, 29.0108)^T \text{ rad/s}$$

and

$$\pm\,(0.0727, -2.1084, 0.0, -12.5467)^T \text{ rad/s}$$

Figure 3 shows controlled trajectories in the angular momentum space, with PNC1 beginning near the four unstable equilibria (marked with circles). Each trajectory successfully reaches a minor-axis spin (marked with squares). As mentioned earlier, however, inverted turns occur in Fig. 3, and a small difference of parameters or the initial condition changes the final direction. Note that PNC1 slightly rotates the unstable equilibrium points and swaps the characteristics of the major and the minor axes of the body just as the linear feedback controller in [2]. The trajectories resemble closed polhode paths from minor and intermediate axes drifting toward the positive and negative major axes, respectively. PNC1, however, changes the converging directions as well as switches and rotates the equilibrium points so that the trajectories with symmetric equilibria converge to the same direction. This is caused by the nonlinear feedback terms in PNC1. The first cases in Fig. 3 need much longer initial excitation time intervals to transition from the major to the minor spin, while the second cases transition much earlier since the second cases start in the vicinity of the repulsive open-loop intermediate axis.

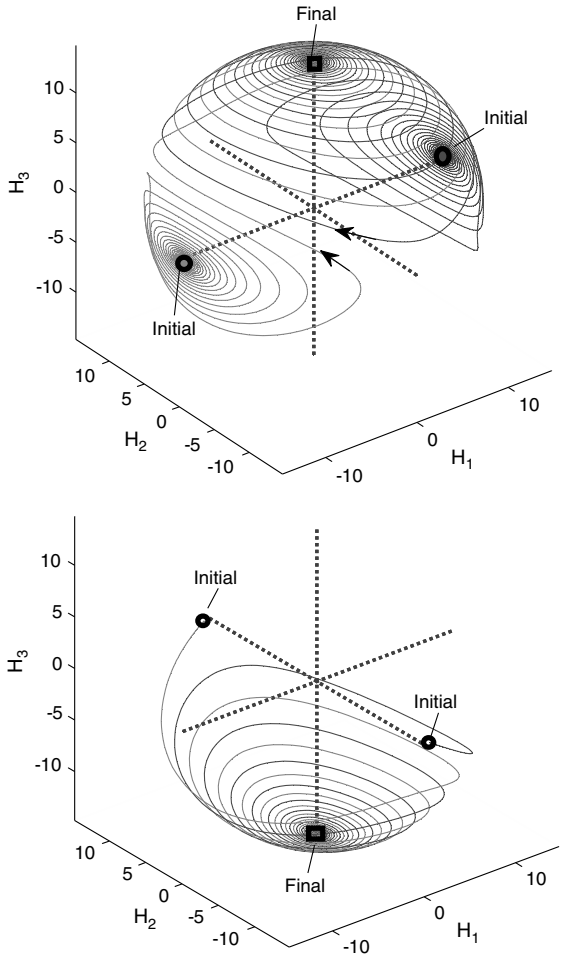

Fig. 3 Nutation control starting near four undesired unstable equilibria by PNC1 (circles, equilibrium points; solid lines, angular momentum trajectories; squares, stable equilibria; dotted lines, principal axes).

Next, a simulation is conducted for a recovery maneuver from the flat-spin condition. The initial condition is set to $\pm(1.8, 0, 0, 0)^T$ rad/s with the same control parameters. PNC1 is compared with a Lyapunov linear feedback control in [12] in this simulation. Performance properties such as the convergence speed, maximum control voltage, and torques become totally different according to the selection of design parameters in both PNC1 and the Lyapunov control. Instead, a comparison reveals interesting characteristics of PNC1 compared with the Lyapunov feedback control. The Lyapunov control is given as

$$e_M = -\kappa(\alpha_1\omega_1 + \alpha_2\omega_2 + \alpha_4\varpi) + N\varpi \tag{29}$$

where κ is an arbitrary constant, and $\alpha_i (i = 1, 2, 4)$ is combined by moments of inertia and θ. The simulation results of PNC1 and the linear feedback control are presented together in Figs. 4 and 5. The feedback gains in Eq. (29) are appropriately chosen to match both transition moments from the major spin to the minor. Figure 4 reveals that PNC1 commands the wheel speed in the opposite direction to Eq. (29) while it achieves the same goal. Also, PNC1 converges faster than Eq. (29) to have much less nutation angle; at 400 s, the nutation angle of PNC1 is less than 0.006 deg, while that of Eq. (29) is about 2 deg, regardless of its final direction. In Fig. 5, the control voltage of PNC1 in the detumbling stage is much less than that of Eq. (29); however, it has a larger peak voltage, and the body angular momentum tends to be less than Eq. (29). In short, PNC1 has better nutation angle reduction performance while its energy consumption is less effective than the linear feedback control.

The body angular momentum magnitude of PNC1 in Fig. 5 is much less than the total angular momentum for most of the simulation time when PNC1 is engaged. The thin dotted lines of the second graph in Fig. 5 are the body energy levels of pure spins about the minimum, intermediate, and maximum axes for the given initial

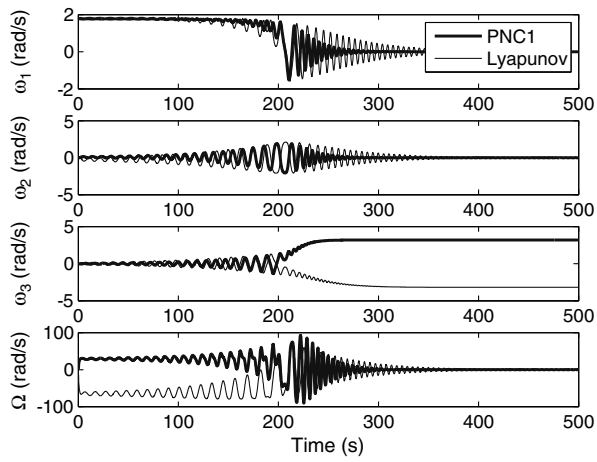

Fig. 4 Angular velocities and the wheel speed for flat-spin recovery by PNC1 and the linear feedback control.

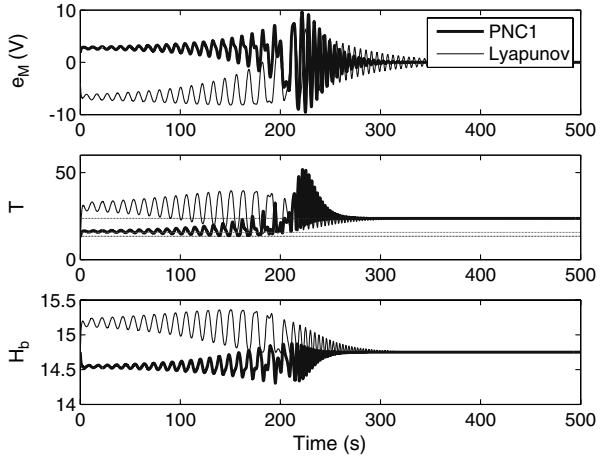

Fig. 5 Control voltage, kinetic energy, and body angular momentum for flat-spin recovery by PNC1 and the linear feedback control.

condition. The kinetic energy of the body is also slightly less than the body minimum energy before transition. Because of this strategy, the control voltage in Fig. 5 imposed during initial excitation is relatively small, and it becomes larger during the transition process. Such characteristics can be mitigated by choosing larger w and smaller h. Also, the convergence after 200 s develops much faster than the excitation before 200 s because PNC1 has the second-order feedback terms, as mentioned earlier. The state variable histories and the control command are totally symmetric for the two opposite initial conditions. The angular momentum trajectories in three-dimensional (3-D) space are illustrated in Fig. 6, beginning in the opposite directions (marked with circles), but both converge to the positive minor-axis spin. Spin polarity after convergence by PNC1 is investigated for various control weights w and prediction intervals h: from 2 to 10 by 0.2 each. Nonconverging cases in 800 s are observed because of the motor input voltage saturation constraint. As seen in Fig. 7, the final spin direction is difficult to be predicted for given parameters. The final direction especially alternates rapidly when h is small, since the ratio of the interval and h itself is even bigger. This behavior means the manifolds converging to each direction are much narrower with these parameters so that the observed spin direction change appears almost chaotic. The extent of chaoticity tends to increase provided the energy dissipation and various types of external torques are considered. Although it is beyond the scope of this paper, [29,30] can be referred to for more study on dynamics and control of chaotic motion of spinning spacecraft. Various initial conditions also give similar results, which were already noticed in [5], even if they are not presented here.

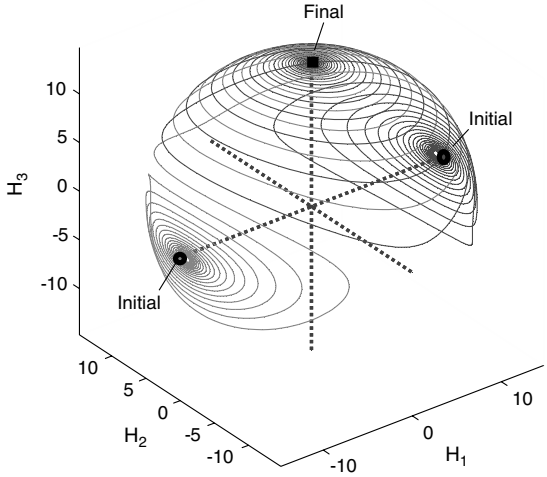

Fig. 6 3-D view of flat-spin recovery by PNC1 starting at two opposite initial conditions (marked with circles).

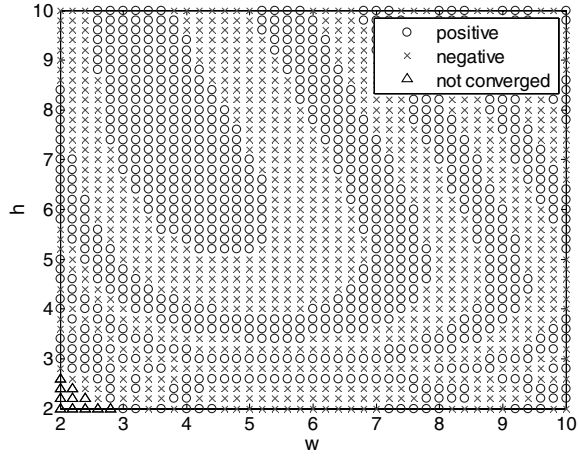

Fig. 7 Final spin direction using PNC1 with various w and h.

B. Design Step 2: Using Outputs of Relative Degrees 1 and 2

To prevent an inverted turn from the spacecraft nutation control, we adopt the dynamics of ω_3 and the minor-axis spin direction command. The output of the system is constructed as

$$y(t) = \begin{bmatrix} \omega_1 \\ \omega_2 \\ \omega_3 \\ \Omega \end{bmatrix} = x(t) \tag{30}$$

Three output variables with the relative degree 1 are controlled directly by the control voltage while ω_3 is excited via nonzero values of the other states. The second-order derivative of ω_3 is obtained as

$$\begin{aligned} I_1 I_2 I_3 \ddot{\omega}_3 &= I_2 \omega_3 \{(I_2 - I_3)(I_1 - I_2)\omega_2^2 + (I_1 - 2I_2 + I_3)K\omega_2 \Omega s\theta \\ &\quad - K^2 \Omega^2 s^2 \theta\} \\ &\quad + I_1 \omega_3 \{-(I_1 - I_3)(I_1 - I_2)\omega_1^2 - (2I_1 - I_2 - I_3)K\omega_1 \Omega c\theta \\ &\quad - K^2 \Omega^2 c^2 \theta\} \\ &\quad + \frac{N}{R}(N\varpi - e_M)\{I_1^2 s\theta \omega_1 - I_2^2 c\theta \omega_2 - (I_1 - I_2)K\Omega s\theta c\theta\} \\ &\triangleq I_1 I_2 I_3 (f_{33} + g_{33} e_M) \end{aligned}$$

The predicted output is expressed as

$$y(t+h) \approx y(t) + \begin{bmatrix} hf_1 \\ hf_2 \\ hf_3 + \frac{h^2}{2} f_{33} \\ hf_4 \end{bmatrix} + \begin{bmatrix} hg_1 \\ hg_2 \\ \frac{h^2}{2} g_{33} \\ hg_4 \end{bmatrix} e_M \tag{31}$$

We also define the output reference trajectory as $r(t) = [0, 0, \omega_{3\text{ref}}(t), 0]^T$, where $\omega_{3\text{ref}}(t)$ will be designed later to drive the spin polarity to a desired direction. Defining the output weight as

$$Q_2 = \begin{bmatrix} I_1^2 & 0 & 0 & 0 \\ 0 & I_2^2 & 0 & 0 \\ 0 & 0 & I_3^2 & 0 \\ 0 & 0 & 0 & K^2 \end{bmatrix}$$

expands the cost function as

$$\begin{aligned} J_2 = \tfrac{1}{2}[&\{I_1 \omega_1 (t+h)\}^2 + \{I_2 \omega_2 (t+h)\}^2 + \{I_3[\omega_3 (t+h) \\ &- \omega_{3\text{ref}}(t+h)]\}^2 + \{K\Omega(t+h)\}^2 + We_M^2] \end{aligned} \tag{32}$$

which still implies a combination of the angular momentum components. But, due to the third term, it seeks a solution minimizing the angular momentum of the body relative to the reference angular momentum in the $\boldsymbol{b}_3$ axis with minimum control input. Consequently, the opposite spin is distinguished and can be avoided.

Adopting the control weight transform in Eq. (18) again and inserting Eq. (31) yields Eq. (15) as

$$e_{M2}(t) = -\frac{R}{N(w+2+h^2 g_{33}^2/4)}\left[\frac{1}{h}(-I_1\omega_1 c\theta - I_2\omega_2 s\theta + K\Omega) - \{(I_2-I_3)\omega_2\omega_3 c\theta + (I_3-I_1)\omega_3\omega_1 s\theta + 2\frac{N^2}{R}\varpi\right\} + \frac{1}{2}\left\{I_3(\omega_3-\omega_{3\text{ref}}^h) + h[(I_1-I_2)\omega_1\omega_2 + K\Omega(\omega_2 c\theta - \omega_1 s\theta)] + \frac{h^2}{2}I_3 f_{33}\right\} g'_{33}\Bigg] \tag{33}$$

where

$$g'_{33} \triangleq \frac{1}{I_1 I_2}\{-I_1^2\omega_1 s\theta + I_2^2\omega_2 c\theta + (I_1-I_2)K\Omega s\theta c\theta\}$$

Let us entitle the control law in Eq. (33) as PNC2. Comparing PNC2 with PNC1 in Eq. (19), PNC2 additionally contains the inverse of the state-dependent feedback gain added to the control weight w and the third- and the fourth-order state feedback terms. A larger prediction step reduces the feedback gain and increases the contribution of the higher-order terms, which drastically boosts nonlinearity in the control law. Interestingly, the predicted output causes more prediction error when the prediction step is longer so that the predicted output intrinsically induces a large feedback gain. In this problem, a tumbling motion is periodic so that terms from the first- and the second-order derivatives inherently generate periodic harmonics magnified in the ratios of h and h^2, respectively. The direct feedback of $\Delta\omega_3$ also makes it possible to control the spin orientation. Since $\omega_{3\text{ref}}^h$ is positive or negative, $\Delta\omega_3$ is larger only when the sign of w_3 is opposite to the desired direction. This extends the capability of this control law to the spin inversion control, since either $+H_0/I_3$ or $-H_0/I_3$ become the exclusive global minimum of the cost function J_2.

1. *Reference Generation for ω_3 Tracking*

The reference trajectory was not defined in the previous section. PNC2 still works if we define $\omega_{3\text{ref}}$ as a desired final value of ω_3 and not as a smooth trajectory, as we did for the other state variables by defining them as zeros. However, due to $\Delta\omega_3$, excessive control input is observed before crossing the separatrix during recovery from a flat spin, even if the overall recovery time is not shorter than that of PNC1 without $\Delta\omega_3$ feedback terms. This implies that a portion of the constant, having zero frequency, of the input contributes little to the initial tumbling motion from the major-axis spin while it determines the final spin polarity. Therefore, a smooth reference trajectory of ω_3 is needed to prevent input saturation, considering its behavior in the flat-spin motion.

State or output reference trajectories in the previous literature [22–25] were designed almost arbitrarily, since spacecraft were equipped with three-axis attitude control function. On the other hand, the behavior of the angular velocities in the spinning spacecraft considered in this study is restricted, because it is controlled only by a single reaction wheel. The controlled angular velocity trajectory possesses a spiral-shaped polhode in the 3-D space, and ω_3 exhibits a sigmoid-shaped time history for which the center is around the moment of transitioning from the major-axis spin to the minor crossing the open-loop body separatrix. But, it is really difficult to predict when crossing will happen, because the transition occurs around the intermediate axis, so that if the curve once misses the transition there, the trajectory traces at least about another half cycle, delaying the transition process for about a half-nutation period and crossing the separatrix in the opposite direction. Therefore, the transition moments are not continuous even if the control design parameters such as the prediction step and the control weight, or even the initial conditions, vary continuously.

Hence, we propose an approach to generate an online reference trajectory for ω_3 rather than using a predesigned history. Since the behavior of ω_3 during flat-spin recovery resembles that of the characteristic parameter in Eq. (11), it is employed for a reference generation. Now, a reference trajectory is proposed as

$$\omega_{3\text{ref}}^{\text{cp}}(t) = \frac{I(t)-I_1}{I_3-I_1}\frac{H_{b0}}{I_3} \tag{34}$$

The behavior of the characteristic parameter is highly nonlinear and difficult to predict. Meanwhile, since the prediction step is usually designed smaller than the transition time interval, we may use the current reference as a predicted one:

$$\omega_{3\text{ref}}(t+h) \approx \omega_{3\text{ref}}^{\text{cp}}(t) \tag{35}$$

Note that the reference trajectory need not satisfy the equation of motion in Eq. (7).

2. *Stability Analysis of the Control Law*

As seen in Eq. (33), PNC2 is highly complicated, so closed-loop system stability is difficult to prove. Instead, equilibrium points on the $\boldsymbol{b}_1\boldsymbol{b}_2$ plane are sought in this section, then convergence and stability will be discussed through numerical studies in the next section.

Equilibrium points are calculated by the same procedure used for PNC1. Equations (20) and (21) are solved for e_{M2} in Eq. (33). First, assuming $\omega_3 = 0$, the parallel angular velocity and momentum condition in Eq. (20) is simplified to Eq. (22), while the stuck wheel condition in Eq. (21) becomes

$$\boldsymbol{\eta}\cdot\boldsymbol{\sigma} = 0 \tag{36}$$

where

$$\begin{aligned}\boldsymbol{\eta} &= (\eta_1,\eta_2,\eta_4)^T \\ &= \Bigg[\left(\frac{I_1}{h}+\frac{wN^2}{R}\right)c\theta - \omega_{3\text{ref}}^h\frac{I_1I_3}{2I_2}s\theta, \\ &\quad \left(\frac{I_2}{h}+\frac{wN^2}{R}\right)s\theta + \omega_{3\text{ref}}^h\frac{I_2I_3}{2I_1}c\theta, \\ &\quad -\left(\frac{K}{h}+\frac{wN^2}{R}\right) + \omega_{3\text{ref}}^h\frac{(I_1-I_2)I_3K}{2I_1I_2}c\theta s\theta\Bigg]^T\end{aligned}$$

Solving Eqs. (22) and (36) gives

$$\sigma_1^2\eta_1 s\theta + \sigma_1\sigma_2\left\{-\eta_1 c\theta + \eta_2 s\theta + \eta_4\frac{(I_1-I_2)}{K}\right\} - \sigma_2^2\eta_2 c\theta = 0 \tag{37}$$

Unlike for PNC1, Eq. (37) has real roots when

$$\left(\eta_1 c\theta - \eta_2 s\theta - \eta_4\frac{I_1-I_2}{K}\right)^2 + 4\eta_1\eta_2 c\theta s\theta \geq 0 \tag{38}$$

If Eq. (37) has imaginary solutions, there is no equilibrium point on the $\boldsymbol{b}_1\boldsymbol{b}_2$ plane. The orthogonal vector $\boldsymbol{\eta}$ of PNC2 deviates due to $\omega_{3\text{ref}}^h$ from $\boldsymbol{\eta}$ of PNC1. Under the condition of Eq. (38), $\sigma_i = \mu_i\sigma_2$ and $\sigma_i = \nu_i\sigma_2$ $(i = 1,\ 4)$. We again arrive at the solutions: $\pm(\mu_1\sigma_2, \sigma_2, 0, \mu_4\sigma_2)^T$ and $\pm(\nu_1\sigma_2, \sigma_2, 0, \nu_4\sigma_2)^T$.

When $\omega_3 \neq 0$, since $\dot{\Omega} = 0$, Eq. (20) is rewritten as

$$\frac{I_1\sigma_1 + K\sigma_4 c\theta}{\sigma_1} = \frac{I_2\sigma_2 + K\sigma_4 s\theta}{\sigma_2} = I_3 \tag{39}$$

Simplifying Eq. (21) with Eq. (22) and substituting Eq. (39), it follows that

$$\sigma_4\left\{\frac{1}{h}\left(\frac{I_1c^2\theta}{I_1-I_3}+\frac{I_2s^2\theta}{I_2-I_3}+1\right) + \frac{N^2w}{R}\left(\frac{1}{K}+\frac{c^2\theta}{I_1-I_3}+\frac{s^2\theta}{I_2-I_3}\right) + (\sigma_3-\omega_{3\text{ref}}^h)\frac{I_3}{2I_1I_2}\left(\frac{I_1^2}{I_1-I_3}-\frac{I_2^2}{I_2-I_3}+I_1-I_2\right)s\theta c\theta\right\} = 0$$

Thus, since $\sigma_3 \leq H_0/I_3$, if

$$\left|\omega_{3\text{ref}}^{h} - \frac{1/h\{[(I_1c^2\theta)/(I_1-I_3)]+[(I_2s^2\theta)/(I_2-I_3)]+1\}+[(N^2w)/R]\{(1/K)+[c^2\theta/(I_1-I_3)][c^2\theta/I_1-I_3)]+[s^2\theta/(I_2-I_3)]\}}{I_3/2I_1I_2\{[I_1^2/(I_1-I_3)]-[I_2^2/(I_2-I_3)]+I_1-I_2\}s\theta c\theta}\right|$$
$$= |\omega_{3\text{ref}}^{h} - \bar{\sigma}_3| > \frac{H_0}{I_3}$$

$\sigma_4 = 0$, and $(0, 0, \pm H_0/I_3, 0)^T$ are the only equilibrium points. In fact, for the parameters in Table 1, $\bar{\sigma}_3 = -1112.7$ rad/s.

Consequently, there exist six equilibrium points including the desired final state. Stability of the six equilibrium points will be discussed with the numerical simulation results in the following section. Unlike for PNC1, the former four equilibria in this case and the opposite point to the desired spin are unstable, and stable is the only desired condition.

3. *Numerical Examples*

Because of the complexity of the closed-loop dynamics of spacecraft with the predictive nutation controller, the essentially global convergence of the system with PNC2 is addressed by numerical examples. Simulation parameters and conditions identical to those in the previous section are used. The four undesired equilibria are obtained as

$$\pm\,(1.8458, -0.2584, 0.0, -74.2517)^T \text{ rad/s}$$

and

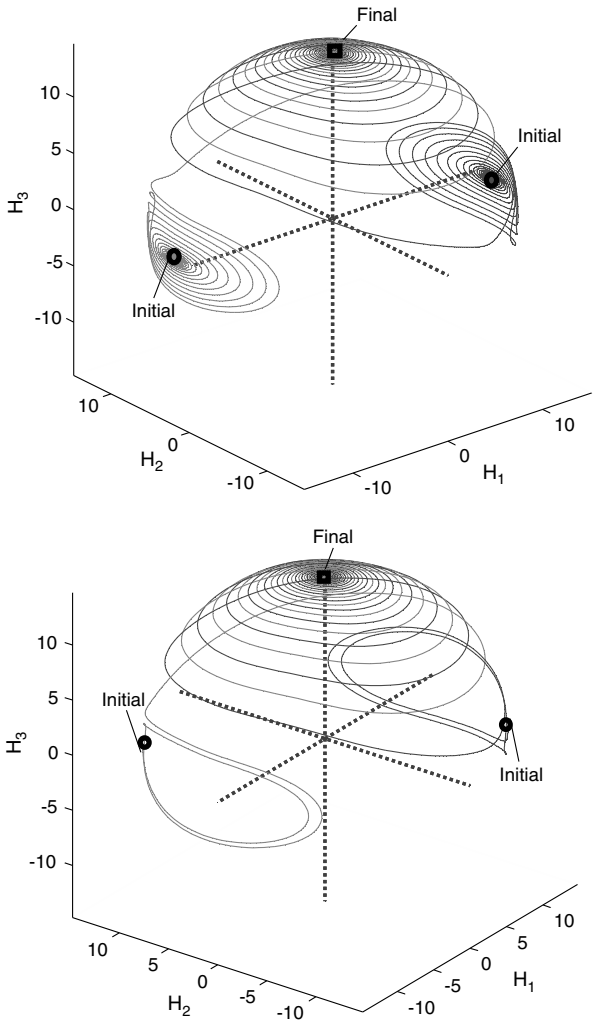

Fig. 8 Nutation control starting near four undesired equilibria by PNC2 (circles, equilibrium points; squares, stable equilibrium).

$$\pm\,(1.2380, -1.5973, 0.0, -159.1621)^T \text{ rad/s}$$

Nutation control trajectories starting near the four equilibria on the $\boldsymbol{b}_1\boldsymbol{b}_2$ plane are presented in Fig. 8, which verifies the four undesired equilibria are dynamically unstable. It is noted that the third and the fourth unstable equilibria have moved considerably toward the first and the second, respectively, by PNC2, otherwise located in the vicinity of the body intermediate axis. As a result, they trace one swing around the body major axis, just as the trajectories of the other two. This means the control law of PNC2 in Eq. (33) distorts the stable manifolds on the ellipsoid and merges the polhode paths initially toward the negative minor axis to those toward the positive minor axis. Therefore, unlike in Fig. 3, the four trajectories converge to the positive spin for $\omega_{3\text{ref}} = H_0/I_3$. This phenomenon is partially observed in PNC1 as well. In the 3-D view of PNC1 in Figs. 3 and 6, it can be seen that the two paths mingle in the spiral shapes from the opposite equilibria toward the same direction. This implies that PNC1 breaks the symmetry of the open-loop system manifolds about the origin and rearranges the convergence polarity of the closed-loop manifolds, unlike the linear control in [2].

Recovery from the flat-spin condition is also simulated. Figure 9 compares simulation results with two different references: case 1) thin lines for $\omega_{3\text{ref}} = H_0/I_3$ and case 2) thick lines for the online time-varying reference of Eq. (34). The spin transition of case 2 is completed in about 150 s, while that of case 1 is completed in about 200 s. Case 1 imposes much more control input on the system during initial excitation so that the wheel speed saturates around -100 rad/s due to control voltage saturation. The smooth online reference trajectory reduces control input and torques with faster transition. Compared with PNC1, PNC2 tends to generate more input voltage and exhibits correspondingly faster convergence, as seen in Fig. 10. When a smaller maximum control voltage is allowed, we may select smaller h and larger w, which tend to slow down the convergence speed and reduce the maximum input. Because PNC2 with a small h behaves just as PNC1, it enables more design flexibility in the control law than PNC1. Figure 11 depicts angular momentum trajectories beginning on the two opposite major-axis spin conditions marked with circles, which are also perfectly symmetric. In Fig. 12, the nutation angles are presented in the logarithmic scale altogether: Lyapunov control, PNC1, and PNC2 with the constant and the online references. The nutation angle of PNC2 with the online reference

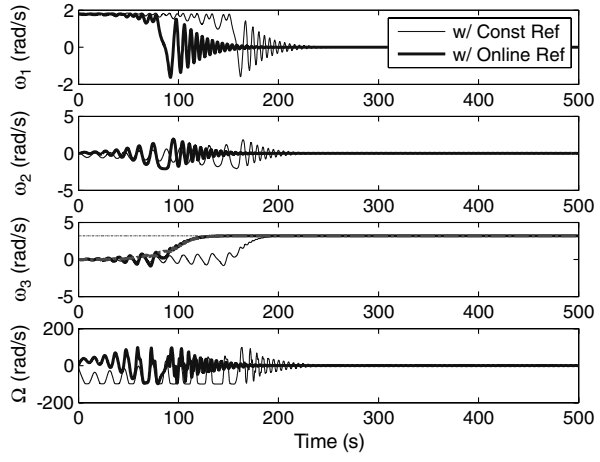

Fig. 9 Angular velocities and wheel speeds for flat-spin recovery by PNC2 with a final value reference (thin broken lines) and with the online time-varying reference (thick broken line).

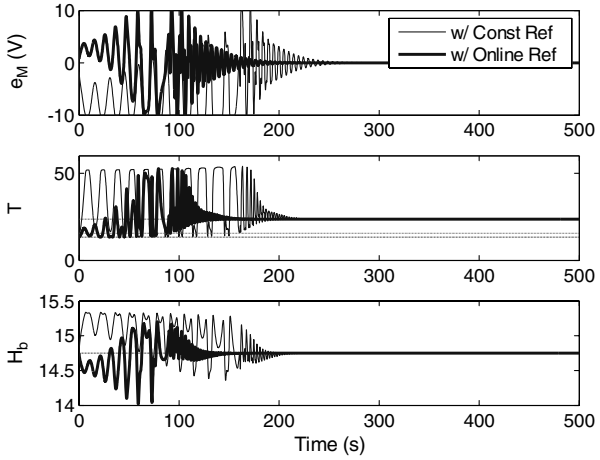

Fig. 10 Control voltage, kinetic energy, and body angular momentum for flat-spin recovery by PNC2 with constant and online references.

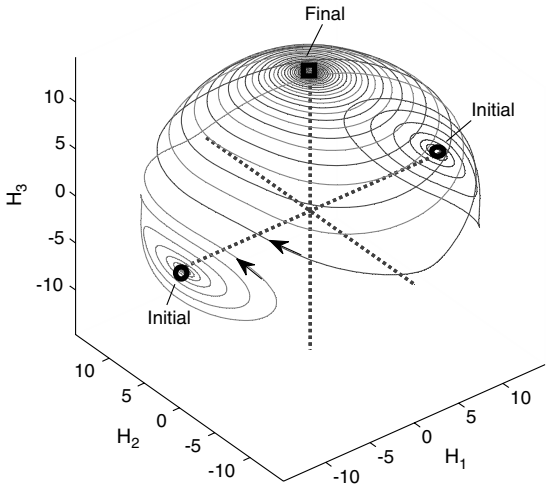

Fig. 11 3-D view of flat-spin recovery by PNC2 with the online reference starting at two opposite initial conditions (marked with circles).

after 450 s is not given due to numerical accuracy limit of the digit. For convenience of comparison, the nutation angle for the Lyapunov control was calculated with respect to the negative spin axis. The decreasing ratio of the Lyapunov control is much slower than that of the other PNCs. PNC2, however, interestingly shows a similar

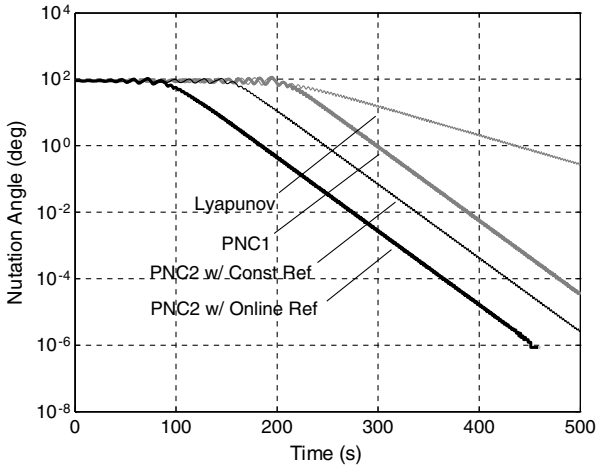

Fig. 12 Nutation angles of Lyapunov control, PNC1, and PNC2 with the constant and the online references in the logarithmic scale.

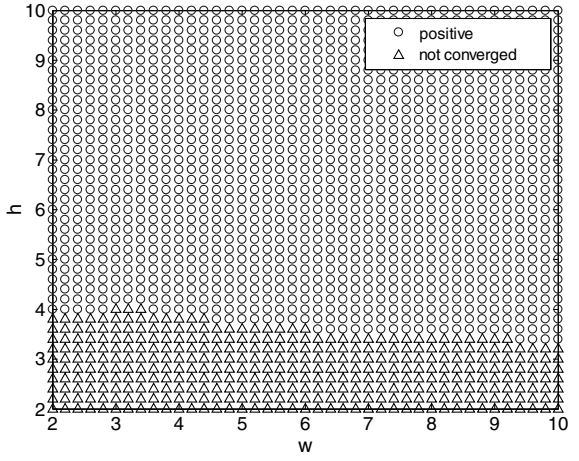

Fig. 13 Final spin direction using PNC2 with various *w* and *h*.

convergence speed with PNC1 once PNC2 transitions to the desired spin direction. The online reference also only accelerates the escape from the flat spin.

Polarity control of PNC2 is verified for various w and h in Fig. 13. Because PNC2 exerts more input, and the control saturation limit is assumed, the nonconverging parameter conditions are increased. Meanwhile, every converging direction is shown to be the positive about the minor axis under a positive $\omega_{3\text{ref}}$.

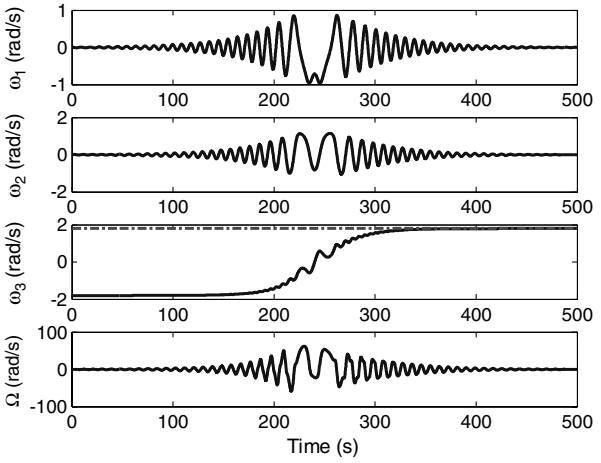

Fig. 14 Angular velocities and the wheel speed of spin inversion by PNC2 with a constant reference.

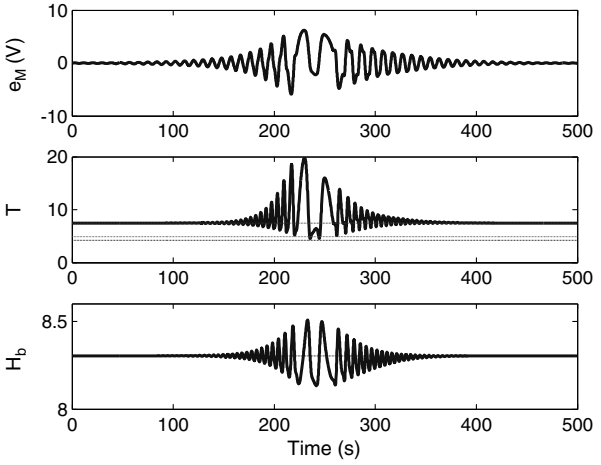

Fig. 15 Control voltage, kinetic energy, and body angular momentum of spin inversion by PNC2.

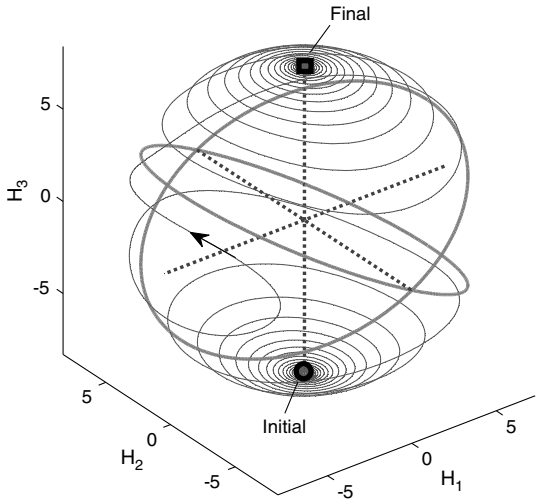

Fig. 16 3-D view of spin inversion by PNC2 with separatrices (thick solid lines).

We now present a spin inversion maneuver by PNC2 with $x_0 = (0.01, 0.0, -1.8, 0.0)^T$ rad/s. In the case of the exact pure spin about the minor axis in the negative direction, the transverse wheel cannot control the vehicle to change its orientation due to unstable equilibrium. It is, however, easily perturbed by an arbitrary wheel spin or external disturbance torques. The reference is defined as $r(t) = (0, 0, H_0/I_3, 0)^T$. Defining $\omega_{3\text{ref}}(t) = H_0/I_3$ is the key to make the negative axis spin unstable and the positive minor-axis spin stable. In Fig. 14, ω_3 increases from the negative to the positive command. All the states and variables in Fig. 15 are almost symmetric around when $\omega_3 = 0$. A 3-D view of the angular momentum trace is visualized in Fig. 16 with body separatrices crossing in the vicinity of the intermediate axis.

In the problem description, it is assumed that the wheel is orthogonal to the desired spin axis and that the spacecraft moment of inertia is perfectly known. To investigate the robustness of the control law, numerous simulations are conducted for a variety of system model errors. It is summarized in Tables 2–4 whether the systems

Table 2 Robustness test case 1: $\theta_{\text{true}}/\theta$

	0.5	0.8	1.5	2.0
PNC1	Converged	Converged	Converged	Converged
PNC2	Converged	Converged	Converged	Converged

Table 3 Robustness test case 2: wheel misalignment out of the b_1b_2 plane (deg)

	−20	−9	9	20
PNC1	Converged	Converged	Converged	Converged
PNC2	Nonconverged	Converged	Converged	Converged

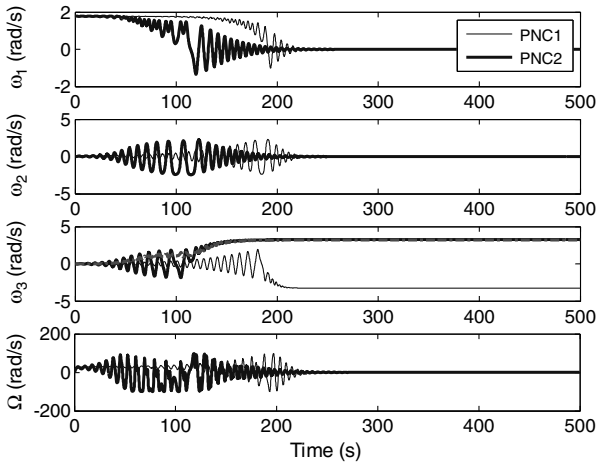

Fig. 17 Angular velocities and the wheel speed for flat-spin recovery by PNC1 and PNC2 under system uncertainties.

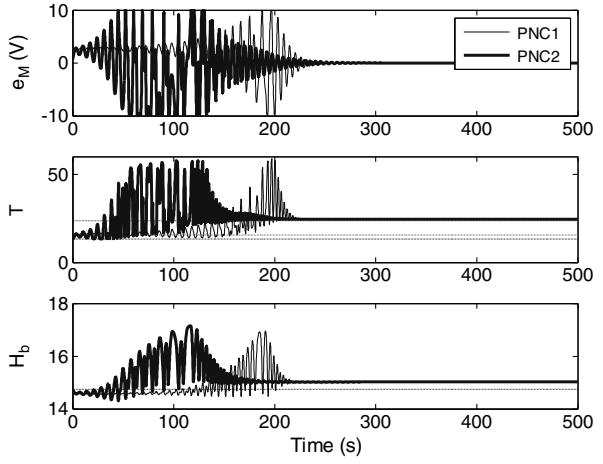

Fig. 18 Control voltage, kinetic energy, and angular momentum for flat-spin recovery by PNC1 and PNC2 under system uncertainties.

with PNC1 and PNC2 converge when recovering from the flat spin in 800 s with identical control parameters under various system uncertainties. PNC1 is considered as convergent when either of the positive or negative spins are achieved. As shown in case 1 of Table 2, both PNC1 and PNC2 are not sensitive to the error of the alignment angle itself. Meanwhile, PNC1 in case 2 converges for a wider range of out-of-plane misalignment of the reaction wheel than PNC2. This characteristic is more evident for uncertainties of the moment of inertia. PNC1 is convergent in all cases as long as $I_{3\text{true}}$ is the actual minor axis. When $I_{2\text{true}}/I_2 = 0.6$, the actual minor axis changes to I_2 from I_3, and PNC1 does not converge. On the other hand, the convergence region of PNC2 is largely restricted. PNC2 in a nonconverging case results in nonexcited or anomalously resonant

Table 4 Robustness test case 3: moment-of-inertia errors

	0.6	0.9	1.1	1.5
		$I_{1\text{true}}/I_1$		
PNC1	Converged	Converged	Converged	Converged
PNC2	Nonconverged	Converged	Nonconverged	Nonconverged
		$I_{2\text{true}}/I_2$		
PNC1	Nonconverged	Converged	Converged	Converged
PNC2	Nonconverged	Nonconverged	Converged	Nonconverged
		$I_{3\text{true}}/I_3$		
PNC1	Converged	Converged	Converged	Converged
PNC2	Converged	Converged	Converged	Nonconverged

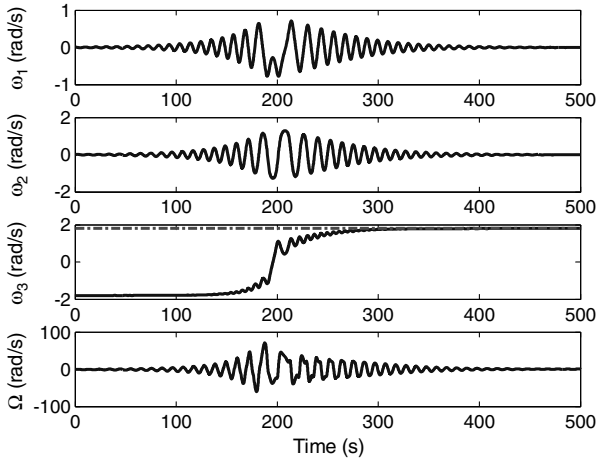

Fig. 19 Angular velocities and the wheel speed for spin inversion by PNC2 under system uncertainties.

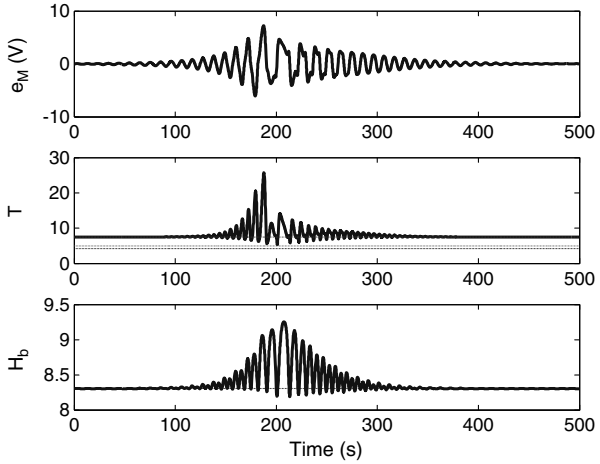

Fig. 20 Control voltage, kinetic energy, and angular momentum for spin inversion by PNC2 under system uncertainties.

states, which is considered due to the complexity and polarity distinction of PNC2.

Finally, we present a simulation result under combined system uncertainties. It is assumed that $\theta_{\text{true}}/\theta = 1.1$, the wheel orientation is 10 deg out of the $\boldsymbol{b}_1\boldsymbol{b}_2$ plane, and $I_{1\text{true}} = 1.1I_1$, $I_{2\text{true}} = 0.95I_2$, and $I_{3\text{true}} = 1.08I_3$ [2]. The following simulation results demonstrate the robustness of PNC1 and PNC2 against system uncertainties for both flat-spin recovery and spin inversion, as shown in Figs. 17–20. Because of uncertainties, tumbling and converging times of PNC2 are elongated with more control input while those of PNC1 shorten a little. It is noted the final body angular momentum is larger than the nominal value in Fig. 18. The spin inversion maneuver, however, does not show much difference from the case without uncertainties, since the required excitation level of kinetic energy is lower, as shown in Figs. 19 and 20, than in the flat-spin case.

V. Conclusions

This paper presented an integrated approach to nutation and spin inversion control problems by means of a predictive control for spin-stabilized spacecraft about the minor axis with a single transverse wheel. Since the nutational motion is determined by the ratio of the angular momentum and the kinetic energy, the predictive cost function to be minimized was designed in the dimension of angular momentum. Then, a two-step strategy was applied to achieve this goal: in the first step, a nonlinear feedback control law was designed to reduce undesired angular momentum components. In the second step, the control law was augmented with desired axis polarity terms using the explicit map between the control and the minor-axis angular velocity, which extended the controllable nutation angle to nearly 180 deg. Design parameters of the predictive control, such as the output and the control weights, the prediction horizon, and reference trajectories, were newly designed and constructed correspondingly.

Analysis and numerical studies disclosed that two parameters can be designed freely for desired convergence speeds and shapes: the prediction time step and the nondimensionalized control weight. Properly selected, the nonlinear predictive control may act as a linear or even a highly nonlinear control, which enables various voltage and control torque profiles.

Investigating behaviors in the vicinity of the equilibrium points revealed that the proposed nonlinear control laws switch the minor- and the major-axis convergence properties and rearrange the stable polhode paths to the minor axis. Furthermore, the second controller reconstructs all the spiral polhode paths toward the desired minor axis by distorting the stable manifolds. It was shown essentially globally stable to a desired spin polarity, including flat-spin recovery and the spin orientation inversion maneuver. Simulation results further demonstrated the robustness of the proposed predictive nutation control against system uncertainties, such as the moment of inertia and the wheel alignment errors.

Acknowledgment

This research was supported by the National Space Laboratory program through the Korea Science and Engineering Foundation funded by the Ministry of Education, Science, and Technology (S10801000123-08A0100-12310).

References

[1] Wertz, J. R. (ed.), *Spacecraft Attitude Determination and Control*, D. Reidel, Dordrecht, The Netherlands, 1978, Chap. 15.

[2] Lawrence, D. A., and Holden, T. E., "Essentially Globally Asymptotically Stable Nutation Control Using a Single Reaction Wheel," *Journal of Guidance, Control, and Dynamics*, Vol. 30, No. 6, 2007, pp. 1783–1793. doi:10.2514/1.27790

[3] Beachley, N. H., and Uicker, J. J., Jr., "Wobble-Spin Technique for Spacecraft Inversion and Earth Photography," *Journal of Spacecraft and Rockets*, Vol. 6, No. 3, 1969, pp. 245–248. doi:10.2514/3.29580

[4] Beachley, N. H., "Inversion of Spin-Stabilized Spacecraft by Mass Translation-Some Practical Aspects," *Journal of Spacecraft and Rockets*, Vol. 8, No. 10, 1971, pp. 1078–1080. doi:10.2514/3.30349

[5] Rahn, C. D., and Barba, P. M., "Reorientation Maneuver for Spinning Spacecraft," *Journal of Guidance, Control, and Dynamics*, Vol. 14, No. 4, 1991, pp. 724–728. doi:10.2514/3.20705

[6] Fong, H. S., Hughes Aircraft Co., Los Angeles, U. S. Patent "Essentially Passive Method for Inverting the Orientation of a Dual Spin Spacecraft," No. 5067673, 26 Nov. 1991.

[7] Devey, W. J., Field, C. F., and Flook, L., "An Active Nutation Control System for Spin Stabilized Satellite," *Automatica*, Vol. 13, No. 2, 1977, pp. 161–172. doi:10.1016/0005-1098(77)90040-1

[8] Fowell, R. A., Milford, R. I., and Yocum, J. F., "Spacecraft Spin Stabilization Using a Transverse Wheel for Any Inertia Ratio," *Journal of Guidance, Control, and Dynamics*, Vol. 22, No. 6, 1999, pp. 768–775. doi:10.2514/2.4477

[9] Bang, H., Myung, H. -S., and Tahk, M. J., "Nonlinear Momentum Transfer Control of Spacecraft by Feedback Linearization," *Journal of Spacecraft and Rockets*, Vol. 39, No. 6, 2002, pp. 866–873. doi:10.2514/2.3909

[10] Seo, I. -H., Leeghim, H., and Bang, H., "Nonlinear Momentum Transfer Control of a Gyrostat with a Discrete Damper Using Neural Networks," *Acta Astronautica*, Vol. 62, Nos. 6–7, 2008, pp. 357–378. doi:10.1016/j.actaastro.2008.01.014

[11] Lian, B., and Bang, H., "Momentum Transfer-Based Attitude Control of Spacecraft with Backstepping," *IEEE Transactions on Aerospace and Electronic Systems*, Vol. 42, No. 2, 2006, pp. 453–463. doi:10.1109/TAES.2006.1642563

[12] Marshall, A., and Tsiotras, P., "Spacecraft Angular Velocity Stabilization Using a Single-Gimbal Variable Speed Control Moment Gyro," AIAA Guidance, Navigation and Control Conference, AIAA Paper 2003-5654, Aug. 2003.
[13] Zhang, H. -H., Wang, F., and Trivailo, P. M., "Spin-Axis Stabilization of Underactuated Rigid Spacecraft Under Sinusoidal Disturbance," *International Journal of Control*, Vol. 81, No. 12, 2008, pp. 1901–1909.
doi:10.1080/00207170801930217
[14] Holden, T. E., and Lawrence, D. A., "A Lyapunov Design Approach to Nutation Damping with a Reaction Wheel," AIAA Guidance, Navigation and Control Conference, AIAA Paper 2000-4047, Aug. 2000.
[15] Fowell, R. A., U. S. Patent "Satellite Spin Inversion Using a Single Degree of Freedom Momentum Storage Device," No. 5758846, Hughes Electronics Corp., Los Angeles, CA, 2 June 1998.
[16] Hall, C. D., and Rand, R. H., "Spinup Dynamics of Axial Dual-Spin Spacecraft," *Journal of Guidance, Control, and Dynamics*, Vol. 17, No. 1, 1994, pp. 30–37.
doi:10.2514/3.21155
[17] Kang, J. -Y., and Cochran, J. E., Jr., "Resonant Motion of a Spin-Stabilized Thrusting Spacecraft," *Journal of Guidance, Control, and Dynamics*, Vol. 27, No. 3, 2004, pp. 356–364.
doi:10.2514/1.10331
[18] Tsui, R., and Hall, C. D., "Resonance Capture in Unbalanced Dual-Spin Spacecraft," *Journal of Guidance, Control, and Dynamics*, Vol. 18, No. 6, 1995, pp. 1329–1335.
doi:10.2514/3.21549
[19] Hall, C. D., "Escape from Gyrostat Trap States," *Journal of Guidance, Control, and Dynamics*, Vol. 21, No. 3, 1998, pp. 421–426.
doi:10.2514/2.4275
[20] Avanzini, G., de Matteis, G., and Petritoli, P., "Numerical Continuation of Torque Free Motions of Gyrostats," AIAA/AAS Astrodynamics Specialist Conference and Exhibit, AIAA Paper 2004-5206, Aug. 2004.
[21] Sandfry, R. A., and Hall, C. D., "Steady Spins and Spinup Dynamics of Axisymmetric Dual-Spin Satellites with Dampers," *Journal of Spacecraft and Rockets*, Vol. 41, No. 6, 2004, pp. 948–955.
doi:10.2514/1.11014
[22] Lu, P., "Nonlinear Predictive Controllers for Continuous Systems," *Journal of Guidance, Control, and Dynamics*, Vol. 17, No. 3, 1994, pp. 553–560.
doi:10.2514/3.21233
[23] Crassidis, J. L., Markley, F. L., Anthony, T. C., and Andrews, S. F., "Nonlinear Predictive Control of Spacecraft," *Journal of Guidance, Control, and Dynamics*, Vol. 20, No. 6, 1997, pp. 1096–1103.
doi:10.2514/2.4191
[24] Singh, S. N., Steinberg, M., and DiGirolamo, R. D., "Nonlinear Predictive Control of Feedback Linearizable Systems and Flight Control System Design," *Journal of Guidance, Control, and Dynamics*, Vol. 18, No. 5, 1995, pp. 1023–1028.
doi:10.2514/3.21500
[25] Myung, H. -S., and Bang, H., "Nonlinear Predictive Attitude Control of Spacecraft under External Disturbances," *Journal of Spacecraft and Rockets*, Vol. 40, No. 5, 2003, pp. 696–699.
doi:10.2514/2.6896
[26] Hughes, P. C., *Spacecraft Attitude Dynamics*, Wiley, New York, 1986.
[27] Sidi, M. J., *Spacecraft Dynamics and Control*, Vol. 7, Cambridge Aerospace Series, Cambridge Univ. Press, New York, 1997.
[28] Or, A. C., "Dynamics of an Asymmetric Gyrostat," *Journal of Guidance, Control, and Dynamics*, Vol. 21, No. 3, 1998, pp. 416–420.
doi:10.2514/2.4274
[29] Kuang, J., Tan, S., Arichandran, K., and Leung, A. Y. T., "Chaotic Dynamics of an Asymmetric Gyrostat," *International Journal of Non-Linear Mechanics*, Vol. 36, No. 8, 2001, pp. 1213–1233.
doi:10.1016/S0020-7462(00)00091-3
[30] Meehan, P. A., and Asokanthan, S. F., "Control of Chaotic Instabilities in a Spinning Spacecraft with Dissipation Using Lyapunov's Method," *Chaos, Solitons and Fractals*, Vol. 13, No. 9, 2002, pp. 1857–1869.
doi:10.1016/S0960-0779(01)00203-X

M. Costello
Associate Editor